BULLETIN OF THE POLISH ACADEMY OF SCIENCES
TECHNICAL SCIENCES, Vol. 72(6), 2024, Article number: e150336
DOI: 10.24425/bpasts.2024.150336

Verification of MLP network-based current sensor fault classifier for vector-controlled AC motor drives

Krystian TELER, Maciej SKOWRON and Teresa Orlowska-Kowalska*

Wroclaw University of Science and Technology, Department of Electrical Machines, Drives and Measurements, Wrocław, Poland

Abstract. In modern drive systems, the aim is to ensure their operational safety. Damage can occur not only to the components of the motor itself but also to the power electronic devices included in the frequency converter and sensors in the measurement circuit. Critical damage to the electric drive that makes its further exploitation impossible can be prevented by using fault-tolerant control (FTC) algorithms. These algorithms are very often combined with diagnostic methods that assess the degree and type of damage. In this paper, a fault classification algorithm using an artificial neural network (ANN) is analyzed for stator phase current sensors in AC motor drives. The authors confirm that the investigated classification algorithm works equally well on two different AC motors without the need for significant modifications, such as retraining the neural network when transferring the algorithm to another object. The method uses a stator current estimator to replace faulty sensor measurements in a vector control structure. The measured and estimated currents are then subjected to a classification process using a multilayer perceptron (MLP), which has the advantage of small structure size as compared to deep learning structures. The uniqueness of the method lies in the use of data in the training set that are not dependent on the parameters of a specific motor. Four types of current sensor faults were studied, namely total signal loss, gain error, offset and signal saturation. Simulations were performed in a MATLAB/SIMULINK environment for drive systems with an induction motor (IM) and a permanent magnet synchronous motor (PMSM). The results show that the algorithm correctly evaluates the type of damage in more than 99.6% of cases regardless of the type of motor. Therefore, the results presented here may help to develop universal diagnostic methods that will work on a wide variety of motors.

Keywords: AC motor drives; current sensor faults; fault classification; neural networks; universal fault classifier.

NOMENCLATURE

State variables:

$\mathbf{u}_s$	spatial vector of stator voltage,
$\mathbf{i}_s$, $\mathbf{i}_r$	spatial vectors of stator and rotor currents,
Ψ_s, Ψ_r	spatial vectors of stator and rotor fluxes,
Ψ_f	permanent magnet flux,
t_{em}, t_L	electromagnetic and load torques,
ω_m	angular rotor speed,
$\omega_{s\psi}$	angular synchronous speed of the rotor flux spatial vector,
γ_ψ	angle between rotor flux vector and axis A of the stator winding,
γ_{is}	angle between stator current vector and axis A of the stator winding,
I_m	instantaneous current amplitude,
r_s, r_r	stator and rotor winding resistances,
$l_{\sigma s}$, $l_{\sigma r}$, l_m	stator and rotor leakage inductances and main inductance of IM,
T_M	mechanical time constant,
f_{sN}	nominal frequency,
e_d, e_q	decoupling signals.

Indexes:

ref	reference value,
mea	measured value,
est	estimated value,
N	nominal value,
A, B, C	indexes of components in phase A, B, C coordinate system,
α, β	indexes of components in stationary α, β coordinate system,
d, q	indexes of components in synchronous d, q coordinate system.

Abbreviations for current sensor faults:

NF, OC, G	no fault, open circuit, gain,
OFF, SAT	offset, saturation,
g, offset, sat	value of gain, offset, and saturation.

1. INTRODUCTION

The development of industrial drive systems that provide optimum motion performance of machines with a high dynamic of changing operating conditions requires the application of advanced control structures. In recent years, closed control structures for electric motors have ceased to perform only regulatory functions, but now they also monitor the behavior of the object. This is due to the desire to maintain high reliability of the drive system and to respond quickly to the defects that occur. This issue is related directly to the idea of fault-tolerant control systems (FTC) [1, 2], which can include both electromechanical systems (electric motors) and elements responsible for the flow of information to the control structure (sensors) [3]. Defects that occur in the induction motor (IM) and permanent magnet synchronous motor (PMSM) drives most commonly used

*e-mail: teresa.orlowska-kowalska@pwr.edu.pl

Manuscript submitted 2024-02-14, revised 2024-04-05, initially accepted for publication 2024-04-29, published in November 2024.

© 2024 The Author(s). This is an open access article under the CC BY license (http://creativecommons.org/licenses/by/4.0/)

in industrial applications do not ensure the elimination or nullification of the impact of damage during drive operation. On the other hand, the effects of sensor defects due to interference with the values of variables within the control structure can be reduced by changes in the control algorithm [3]. For this purpose, it is necessary to detect the defect sufficiently quickly (detection), determine its type (classification), and then perform control changes that ensure compensation for the identified defect (compensation) [4, 5].

The fault detection methods for sensors operating in closed-loop control structures presented in the literature involve analytical techniques. This approach is applied to speed [6, 7] and current sensors (CS) and is limited mainly to drives with induction motors [4, 6–9] and less frequently synchronous motors [10]. Analytical methods provide almost instantaneous fault detection and evaluation of the type of fault, but in the cases where the exact nature of the fault is known at the design stage [11]. If the effect of the defect on the control system or measured signals cannot be determined by means of strict rules and relationships, then the use of analytical techniques is severely limited. This fact is of particular importance when the type of machine or its rated parameters change, but also when the analyzed sensor changes (different sensor characteristics). Any interference with the parameters of the control system or its components can result in reduced precision or total inability to assess the technical condition of the sensors.

Despite the differences in IM and PMSM designs, field-oriented control algorithms are not significantly different. In both cases, information on the current values of the phase currents is required. The use of analytical methods based on current samples and the determination of the relationship between them does not ensure the universality of the diagnostic system. This means that a system developed for one machine cannot be used successfully when operating on another object. Therefore, it becomes important to look for universal fault symptoms that ensure correct defect evaluation regardless of the control object used (electric motor).

The development of fully automated fault diagnosis systems for current sensors is currently linked to the use of artificial intelligence methods and, in particular, neural networks (NN) [10]. Nevertheless, it should be clearly emphasized that the NN used should fulfil the assumed functions but also not become a burden on the computing system. Therefore, deep neural structures (DNN) [12, 13] or machine learning techniques [14, 15] described in the literature result in increased demands on the computational capacity of the host system. Nevertheless, their particular advantage is the ability to directly analyze signals without pre-processing [16]. This results in a significant reduction in the reaction time to an emerging fault. However, DNNs require extensive training data sets and a long training process, and they also cause a significant complication in the implementation process of the detection system.

An alternative to computationally expensive DNNs are classical shallow neural structures (SNNs) [4]. They are currently used in FTC systems in fault detection and classification tasks. A special feature of SNNs is the ability to approximate new unknown input samples obtained from a small set of learning data. This makes the implementation process of such networks as a multilayer perceptron (MLP) particularly easy. However, in this case, it is important to properly select the elements of the input vector of the network. It should provide good-quality information on the technical condition of the analysed object (sensors in our case). Additionally, due to the high dynamics of drive systems involving speed changes and variable load torque, the input information should be properly processed. High precision in sensor faults detection will be achieved if the input vector of the neural network is independent of the operating conditions of the motor and its parameters. This issue is strongly related to the universality of the diagnostic system, understood as the preservation of the precision of operation for different objects under varying operating conditions. Currently, this topic is being increasingly associated with the idea of transfer learning [16]. However, it should be clearly emphasised that transfer learning implies an additional process of training the network to use known patterns. In this article, the universality of the developed classification system includes the appropriate development of the input vector in such a manner that a single NN structure can be used for different test objects (IM and PMSM) without an additional training process. This fact is an undoubted advantage of the proposed approach over advanced systems based on deep neural structures. The main contribution of the authors can be characterised as follows:

- The main achievement was the development of a universal fault classification algorithm for stator current sensors in AC motor drives.
- The classification quality results obtained are comparable for the IM drive and the PMSM drive.
- A multilayer perceptron network (MLP) structure with a small size as compared to deep network structures was used as a classifier.
- The neural network does not require retraining when the algorithm is transferred to another object.
- Training data, which are independent of the electric drive parameters and which can be easily synthesised based on mathematical damage models, were used.
- A simulation verification of the performance of the proposed algorithm was carried out.

The article is divided into five sections. Section 2 gives a mathematical description of IM and PMSM motors, and of the mathematical models of current sensor faults used. The investigated vector control structure is also presented and a study of the effect of sensor faults on drive performance is carried out. The next section describes the fault detection, compensation and classification algorithm. Section 4 provides information on the NN structure used for classification and on the training method. Section 5 contains the test results, and the article ends with conclusions in Section 6.

2. PROBLEM DESCRIPTION

2.1. CS faults description

Current sensors (CS) used in vector-controlled electric drives must exhibit high accuracy and be reliable. Shunt resistors and transducers that take advantage of the Hall phenomenon are the

most commonly used. Both provide a good quality-to-price ratio and, thanks to the use of feedback in Hall transducers, allow for the influence of temperature and external magnetic interference on measurement results to be reduced.

Table 1
Mathematical model of CS faults

Type of fault	Mathematical model
No fault (NF)	$f(x) = I_m \sin(x)$
Open circuit (OC)	$f(x) = 0$
Gain (G)	$f(x) = g I_m \sin(x)$
Offset (OFF)	$f(x) = I_m \sin(x) + offset$
Saturation (SAT)	$f(x) = \min(\text{sat}, \lvert I_m \sin(x)\rvert) \operatorname{sign}(\mathrm{I_m}\sin(\mathrm{x}))$

x – an arbitrary function of time and/or frequency

However, despite the accuracy and reliability of these instruments, the possibility of misalignment (gain error, offset error) and failure (total signal loss described as open circuit in this paper) must be taken into account. In addition, in the case of Hall transducers, there is a risk that the permitted measurement ranges are exceeded, so the operating point shifts into the nonlinear region and a magnetic core saturation phenomenon occurs [17]. Table 1 provides a summary of CS faults, together with mathematical models.

2.2. Mathematical models of IM and PMSM

The research carried out focusses on comparing the performance of the proposed fault classifier for stator current sensors in a drive system with IM and PMSM. Since the characteristics of AC machines under field-oriented control were used to develop the classification method, it is therefore necessary to analyze the mathematical models of both types of motors, which were also used in the simulation studies carried out. To write the description of these machines, well-known simplifying assumptions are made regarding the replacement of windings with distributed parameters by windings with concentrated parameters, along with the assumption of constant parameters and sinusoidal distribution of induction in the air gap, and the omission of nonlinear phenomena (magnetic hysteresis, saturation, eddy currents) [18].

The application of the above assumptions allows us to write the mathematical model of electromagnetic circuits of an AC motor in the state equation form (in *per unit* [p.u.] system), in a synchronously rotating reference frame (d-q):

$$T_N \frac{\mathrm{d}}{\mathrm{d}t}\mathbf{x} = \mathbf{A}(\omega_m)\,\mathbf{x} + \mathbf{B}\,\mathbf{u}, \tag{1}$$

with: $\mathbf{x}$ – state vector, $\mathbf{u}$ – input vector, $\mathbf{A}$ – state matrix, $\mathbf{B}$ – input matrix, ω_m – angular velocity of the rotor.

For the alternative current motors (ACM) considered, namely the induction motor (IM) and permanent magnet synchronous motor (PMSM), these state and input vectors, and suitable matrices are expressed in Table 2.

Table 2
Detailed mathematical description of IM and PMSM

Induction motor

$$\mathbf{x} = \operatorname{col}(\mathbf{i}_s, \boldsymbol{\Psi}_r), \tag{2}$$

$$\mathbf{u} = \mathbf{u}_s, \tag{3}$$

$$\mathbf{A}(\omega_m) = \begin{bmatrix} a_1\mathbf{I} & a_2\mathbf{I} + a_3(\omega_s - \omega_m)\mathbf{J} \\ a_4\mathbf{I} & a_5\mathbf{I} - (\omega_s - \omega_m)\mathbf{J} \end{bmatrix}, \tag{4}$$

with:

$$a_1 = -\frac{r_s}{\sigma l_s} - \frac{(1-\sigma)r_r}{\sigma l_r}, \quad a_2 = \frac{l_m r_r}{\sigma l_s l_r^2}, \quad a_3 = \frac{l_m}{\sigma l_s l_r}, \quad a_4 = \frac{l_m r_r}{l_r}, \quad a_5 = -\frac{r_r}{l_r}, \tag{5}$$

$$\mathbf{B} = \frac{1}{l_s}[\mathbf{I} - \omega_m \mathbf{J}], \tag{6}$$

$\mathbf{i}_s = i_{sd} + j i_{sq}$, $\mathbf{u}_s = u_{sd} + j u_{sq}$, $\sigma = (l_s l_r - l_m^2)/(l_s l_r)$, $T_N = 1/(2\pi f_{sN})$,

PMSM

$$\mathbf{x} = \mathbf{i}_s, \tag{7}$$

$$\mathbf{u} = \operatorname{col}(\mathbf{u}_s, \boldsymbol{\Psi}_f), \tag{8}$$

$$\mathbf{A}(\omega_m) = [a_6\mathbf{I} - \omega_m \mathbf{J}], \tag{9}$$

with:

$$a_6 = -\frac{r_s}{l_s}, \tag{10}$$

where:

$$\mathbf{I} = \begin{bmatrix} 1 & 0 \\ 0 & 1 \end{bmatrix}, \quad \mathbf{J} = \begin{bmatrix} 0 & -1 \\ 1 & 0 \end{bmatrix},$$

$$\mathbf{B} = \frac{1}{\sigma l_s}\begin{bmatrix} \mathbf{I} \\ \mathbf{0} \end{bmatrix}, \tag{11}$$

$\mathbf{i}_s = i_{sd} + j i_{sq}$, $\mathbf{u}_s = u_{sd} + j u_{sq}$, $\boldsymbol{\Psi}_f = \operatorname{col}(\Psi_f, 0)$, $|\boldsymbol{\Psi}_f| = \Psi_f$ (equal to PM flux)

Dynamics of the angular speed, ω_m, can be described using the equation of motion:

$$T_M \frac{\mathrm{d}}{\mathrm{d}t}\omega_m = t_{em} - t_L, \tag{12}$$

and the electromagnetic torque for IM is described as follows:

$$t_{em} = \frac{l_m}{l_r}\operatorname{Im}(\boldsymbol{\Psi}_r \times \mathbf{i}_s) = \frac{l_m}{l_r}\left(\Psi_{rd} i_{sq} - \Psi_{rq} i_{sd}\right), \tag{13}$$

and for PMSM, respectively as:

$$t_{em} = \mathrm{Im}\left(\mathbf{\Psi}_s \times \mathbf{i}_s\right) = \left(\Psi_f i_{sq} + \left(l_{sd} - l_{sq}\right) i_{sd} i_{sq}\right). \tag{14}$$

2.3. Field-oriented vector control structure of IM and PMSM

All tests were carried out in a field-oriented control (FOC) structure, which involves controlling the flux and torque by using the components of the stator current vector in the synchronous d-q coordinate system rotating concurrently with the associated rotor flux vector Ψ_r. A schematic diagram of the FOC structure is shown in Fig. 1, highlighting the reference current signal i_{sd}^{ref} and the angle signal γ_Ψ required for the coordinate system transformation.

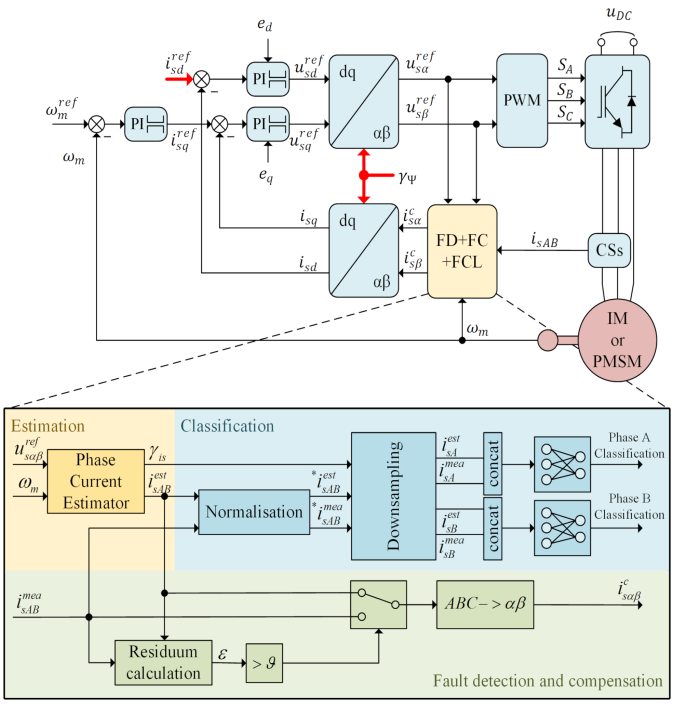

Fig. 1. Schematic diagram of the FOC structure for an IM and PMSM motor including the detection (FD), compensation (FC) and classification (FCL) module

The way in which these signals are determined differs between the structure designed for IM and PMSM. In the case of PMSM, the angle is equivalent to the rotor (and permanent magnets) position angle, while in the case of IM, an estimator of the amplitude and position angle of the flux vector associated with the rotor winding must be used. Improved control quality in the FOC structure using linear PI controllers is achieved by including decoupling signals e_d and e_q, which make the i_{sd} and i_{sq} current control paths independent of each other. These signals are determined from analysis of the stator winding equation in the mathematical model of the motor. Also included in Fig. 1 is the block responsible for implementing the current sensor fault detection, compensation, and classification algorithm (FD+FC+FCL), which will be discussed later in the article.

2.4. Impact of CS faults on drive system performance

The simulations were carried out in a converter system with SVM vector modulation. The FOC control structure used measurements from only two CSs in the calculations, which is common practice in industrial applications. The frequency of the current and speed measurements, the frequency of the PWM carrier signal, and the calculations associated with the control structure were 8 kHz, while the motor dynamics equations were calculated at 800 kHz. The parameters of the motors tested are included in Table 4, in the appendix. The simulations assumed $g = 1.25$, $offset = 0.15 I_m$, and $sat = 0.75 I_m$. The values of these parameters were chosen to show the impact of faults on the performance of the drive. Figures 2–5 show the waveforms of i_{sA}, i_{sB} and i_{sC} phase currents, d-q current components, the electromagnetic torque, and angular velocity when the CS faults being considered occur.

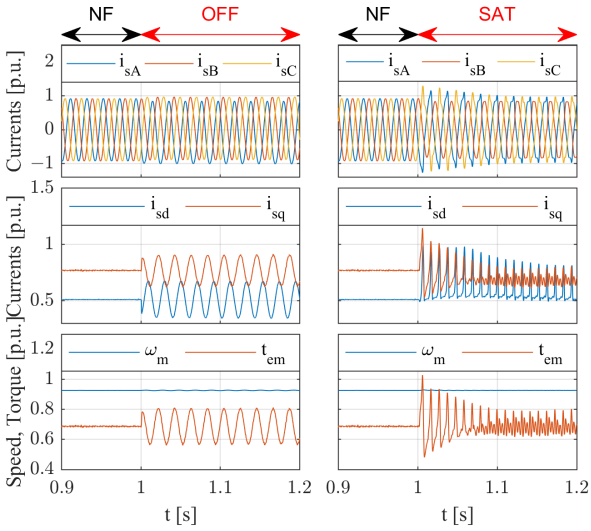

Fig. 2. Waveforms of selected state variables in IM when CS faults (OFF, SAT) occur in phase A ($t_L = t_{LN}$, $\omega_m = \omega_{mN}$)

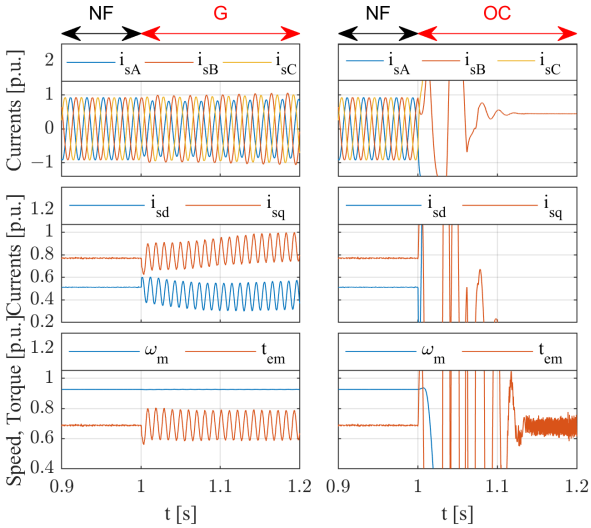

Fig. 3. Waveforms of selected state variables in IM when CS faults (G, OC) occur in phase A ($t_L = t_{LN}$, $\omega_m = \omega_{mN}$)

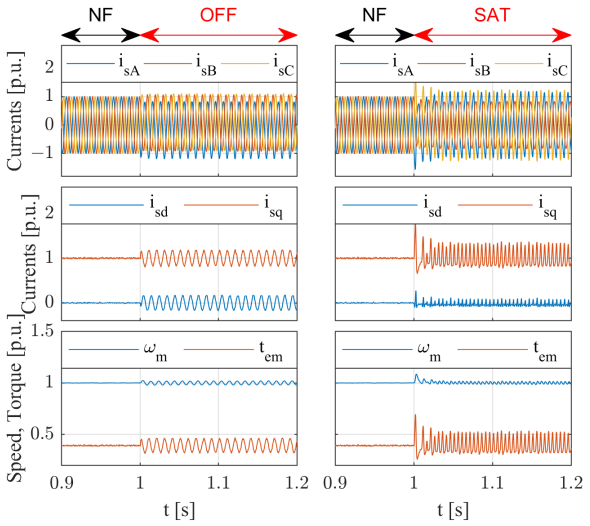

Fig. 4. Waveforms of selected state variables in PMSM when CS faults (OFF, SAT) occur in phase A ($t_L = t_{LN}$, $\omega_m = \omega_{mN}$)

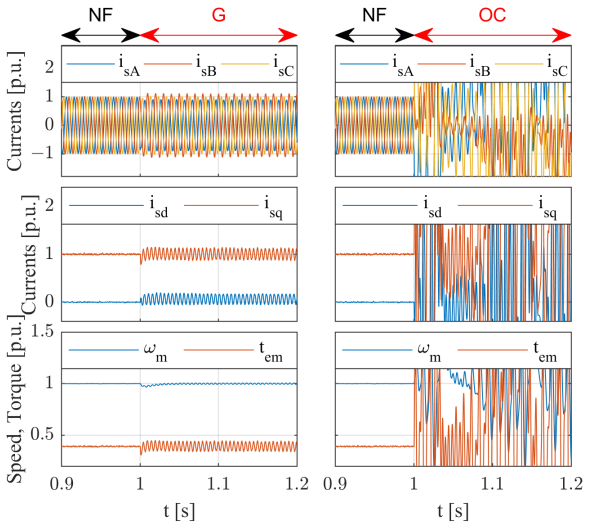

Fig. 5. Waveforms of selected state variables in PMSM when CS faults (G, OC) occur in phase A ($t_L = t_{LN}$, $\omega_m = \omega_{mN}$)

In the case of G and OFF faults, oscillations appear in the current waveforms. These are also noticeable in the electromagnetic torque waveforms, which are proportional to the i_{sq} current. Although the speed is stabilized at a given value, in the real system torque oscillations can lead to accelerated wear of the mechanical parts (rolling bearings) and consequently to serious damage. Furthermore, it should be noted that in the case of G, OFF and SAT faults, ripples appear in the PMSM motor speed (larger than for IM), which increase with the degree of damage. The i_{sd} current, on the other hand, is proportional to the associated rotor flux in the case of IM while in PMSM it is responsible for weakening the flux coming from the permanent magnets. The oscillations of this signal are also significant, resulting in the flux not acquiring a steady-state value, and thus the operating state of the motor can only be described as a quasi-steady state. The most dangerous is the OC-type fault, as measurements from only one CS are then available and, without compensation for this fault, speed control is lost.

Therefore, it is necessary to classify CS damage to decide whether the damage that has occurred is the result of miscalibration or physical damage to the sensor. This can prevent future mechanical faults, which can in turn prove difficult to repair and/or cause considerably more serious production line-related damage, for example.

3. METHODOLOGY OF CS FAULT DETECTION AND CLASSIFICATION

In order to implement the classification, appropriate measurements must first be taken to detect and compensate for CS faults. This action is essential because, as demonstrated in the previous chapter, a sensor fault can cause damage to the drive system. Sufficiently fast detection and compensation will keep the drive system running, which is crucial in fault-tolerant control (FTC) systems.

3.1. Stator current estimators

The classification method developed assumes that an estimator of stator currents is available in the control system. The estimated current values are used for detection and compensation purposes and for fault classification. Therefore, it is important to use an estimator that demonstrates high operating accuracy.

The reconstruction of stator phase currents can be realized using Luenberger observers. This type of solution is very accurate, however, measurements from at least one undamaged sensor are required for operation. When the required measurements are missing, good current reconstruction results are obtained using open-loop observers [8, 19], which were used in this paper. For both motors, these estimators are mathematical models that describe the dynamics of the electromagnetic state variables, in the form of equation (1) and the corresponding equations (2)–(6) for IM or (7)–(11) for PMSM.

3.2. Fault detection and compensation

Early damage detection is performed by comparing the measured and estimated current values (green part in Fig. 1). In the method described in this paper, localization is the task of the neural classifier, so a simple residuum expressed by the following equation is assumed:

$$\varepsilon = \left(i_{sA}^{\text{mea}} - i_{sA}^{\text{est}}\right)^2 + \left(i_{sB}^{\text{mea}} - i_{sB}^{\text{est}}\right)^2. \tag{15}$$

For undamaged sensors, the residuum calculated using the above formula should be zero. However, due to measurement noise and potential discrepancies in the parameters of the current estimator, the value of ε will be non-zero, so it should be compared with the detection threshold, ϑ. It should also be noted that the residuum can have different values at different points of drive operation, so a fixed detection threshold value might not be sufficient in some applications and should then be replaced by an adaptive value [4]. When significant measurement discrepancies occur and the value of ε exceeds the detection threshold, ϑ, the

measuring sensors must be disconnected, and the unavailable measurements replaced by estimated currents (fault compensation). This way, the continuity of control is maintained, and the drive can remain in safe operation.

3.3. Classification

The evaluation of the type of fault is carried out using a neural classifier that compares the values of measured and estimated currents. The assumption of the effectiveness of the classifier is the presence of reproducible fault symptoms in each recorded period of sinusoidal stator current. However, classification of sinusoidal signals is difficult due to the variable frequency and variable amplitude of the signals. Both problems were solved using an available current estimator. Difficulties due to variable amplitude were eliminated by normalizing the signals with respect to the instantaneous amplitude of the estimated current:

$$i_{snA/B}^{\text{mea/est}} = \frac{i_{sA/B}^{\text{mea/est}}}{I_m^{\text{est}}} = \frac{i_{sA/B}^{\text{mea/est}}}{\sqrt{\left(i_{s\alpha}^{\text{est}}\right)^2 + \left(i_{s\beta}^{\text{est}}\right)^2}}. \tag{16}$$

In the above equation, $i_{snA/B}$ denotes the currents normalized in phases A and B, respectively. The variable frequency of the current signal is in turn the result of sampling the measurements at a constant frequency. Therefore, it is proposed to synchronize measurement acquisition with the position angle of the stator current vector. An estimator is also used for this purpose along with the current angle of the stator current vector γ_{is}, determined in the stationary α-β system as follows:

$$\gamma_{is} = \tan^{-1}\left(\frac{i_{s\beta}^{\text{est}}}{i_{s\alpha}^{\text{est}}}\right). \tag{17}$$

If the current samples are always recorded at the same values $\gamma_{is} = \gamma_{\text{acc}}$ then a current waveform independent of the sampling frequency will be obtained. The values of γ_{acc} can be determined from the formula below:

$$\gamma_{\text{acc}} = \gamma_{is0} + k\frac{2\pi}{M-1}, \quad k = 0, 1 \ldots, M-1. \tag{18}$$

In the above formula, γ_{is0} depends on the stator phase in which the measurement acquisition is made and it defines the conventional start of the current period, while M is the assumed number of samples that form one period of the signal.

4. MLP-BASED CLASSIFIER

4.1. Structure of NN-based classifier

In the study, a multilayer perceptron neural network with two hidden layers was used. The mathematical description of such a network is very simple, which allows for easy implementation. Networks of this type are also characterized by relatively high performance with a small learning data set. The input layer contained $2M = 34$ inputs, of which the first $M = 17$ inputs correspond to the measured current signal and the next 17 inputs – to the estimated current signal (Fig. 6). Both signals were subjected to the acquisition process described in Section 3.3. Due to the data normalization performed, the input layer did not contain any additional signal conditioning functions. The hidden layers consisted of $H_1 = 11$ and $H_2 = 3$ neurons, respectively, whose activation functions were a hyperbolic tangent. The output layer was a classifier layer described by a *softmax* function and contained 5 outputs corresponding to the following classes: NF, OC, G, OFF, SAT. The chosen network structure was characterized by the highest accuracy on the learning data prepared as described in the next subsection and, at the same time, contained the lowest number of weight connections.

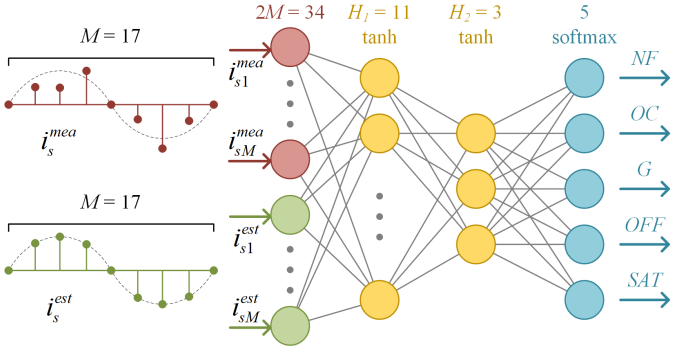

Fig. 6. Schematic diagram of the neural network used

4.2. Training dataset

The process of conditioning the current signals has made it possible to eliminate frequency and amplitude information that is unnecessary from a classification point of view. As a result, and assuming that the mathematical damage models are known, training data can be generated without having to simulate the drive operation.

The process of preparing the training data is based on generating one period of a sinus function waveform consisting of M samples. The basic waveform is then modified on the basis of mathematical models of sensor faults to produce waveforms representing the current signal for different classes and different damage values. To differentiate between the training data, waveforms shadowed by a random variable with normal distribution are also included.

Increasing the generalization capability of the network and making it immune to indicating false predictions was achieved by adding waveforms recorded on the laboratory bench with the IM motor. Additional data represented 20% of the total set. The method of mixing packets derived from the model and measurements of the object used in the study refers to instance-based transfer learning. This technique involves inserting random samples from the target set (the test object) into the training data set of the neural network. Mixing samples from the source set with random samples from the target set helps ensure high performance for unknown input sample networks. The purpose of this paper is to investigate the performance quality of the MLP network developed for IM in a drive system with PMSM, so NN retraining was not performed for a different motor.

5. RESULTS COMPARISON FOR IM AND PMSM

5.1. Simulation conditions

A comparison of the performance of the classifier was carried out by means of simulation in the MATLAB/SIMULINK environment. Four different types of faults (OC, G, OFF, SAT) with values $g = 1.25$, $offset = 0.15I_m$ and $sat = 0.75I_m$ were tested for four different speeds ($\omega_m = \omega_{mN}, 0.75\omega_{mN}, 0.5\omega_{mN}, 0.25\omega_{mN}$) and four load torque values ($t_L = t_{LN}$, $0.75t_{LN}$, $0.5t_{LN}$, $0.25t_{LN}$). The drive system assumed the existence of only two current sensors (in phases A and B), so two simulations were run for each operating point, in which only the selected sensor was damaged. The drive system used the estimated currents to determine control from the start of its operation, so the measured currents had no effect on the performance of the structure. This operation was intended to compare the quality of the classification.

5.2. Signals analysis

The velocity and load torque profiles used in each simulation are shown in Fig. 7a, while examples of measured and estimated currents and classification results for the IM and PMSM motor systems are shown in Fig. 7b and Fig. 7c. In Fig. 7c, significant classification inaccuracies can be observed at times when the PMSM motor was unloaded with any torque (from 0.67 to 0.80 s). The green arrow marks the first current period detected by the classifier, immediately at start-up. It is classified erroneously, which, however, can be negated by software. In Fig. 7c, significant classification inaccuracies can be seen in the instants when the PMSM motor was unloaded (from 0.67 to 0.80 s). These are due to the small value of the current, which is significantly distorted from the assumed sinusoidal waveform under this operating condition. Classification in an unloaded PMSM motor is therefore significantly difficult, but such a motor operating condition is rare and not economically justified. In the case of the IM motor, no-load classification errors do not occur. Nevertheless, during the start-up itself, when the speed rises quite rapidly to the set speed (from 0.33 to 0.67 s), the classification is correct, confirming the robustness of the developed classification method to variations in frequency of the current.

Figure 8 shows an example of classification instants after a SAT fault. Due to the method of measurement acquisition, the correct network response is obtained at the end of the current period. The green rectangle is the result of classification of the period marked by the green arrow, while subsequent current periods are separated by vertical lines in the diagrams. Therefore, the classification time is variable and depends on the fundamental frequency of the current signal in each phase.

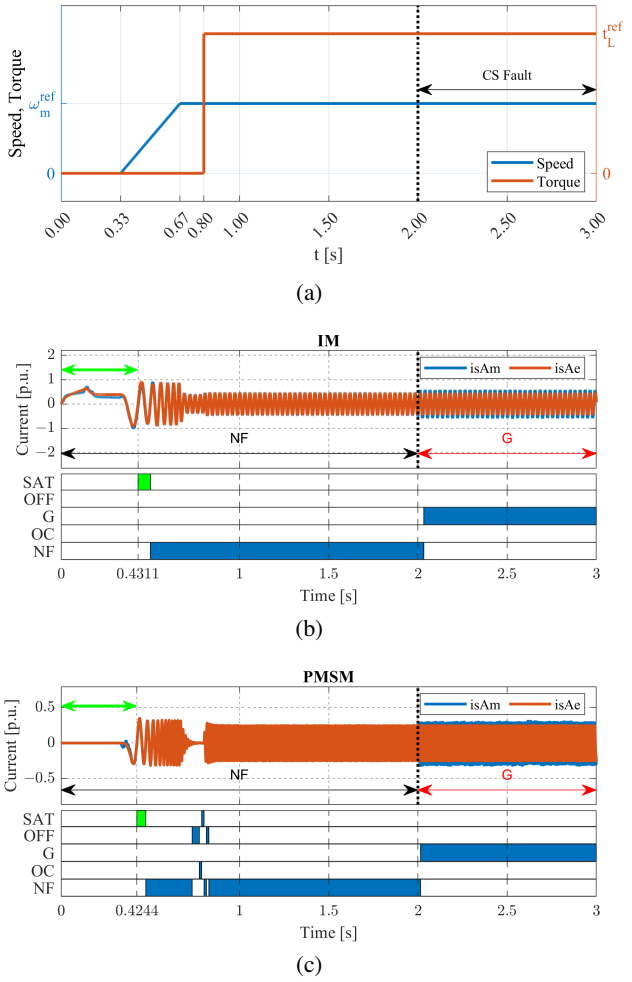

Fig. 7. Waveforms of the set speed and torque and the moment of fault occurrence (a), waveforms of the currents and the classification results in a drive system with an IM motor (b) and a PMSM motor (c) at a speed of $0.75\omega_{mN}$ and a load of $0.25t_{LN}$

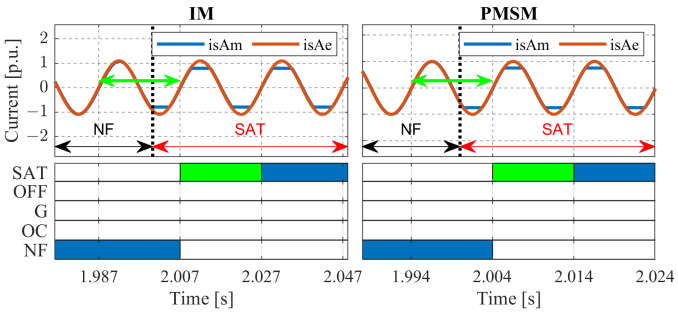

Fig. 8. Classification results for phase A, at nominal speed and nominal torque

5.3. Statistical analysis

Evaluation metrics used to describe the performance of classifiers (Table 3) and the confusion matrix (Fig. 9) were determined from the tests. The calculations included a 2 s simulation for each point of steady-state drive operation (1 s to 3 s), where for the first second of the selected time interval, the CSs were undamaged, and then a sudden failure occurred. The effectiveness (accuracy) of the classifier in the steady state of the drive calculated for IM is 99.6%, while for PMSM it is 99.8%. Such high values are due to the simulation conditions, where the exact parameters of both motors are known, and thus the estimators show high performance accuracy.

Despite the simulation conditions, the results obtained confirm the effectiveness of the method and its versatility. When analyzing the confusion matrix (Fig. 9), it can be seen that when

Table 3
Evaluation metrics describing the classifier under study

Class	IM [%]			PMSM [%]		
	Precision	Recall	F1 score	Precision	Recall	F1 score
No Fault (NF)	99.6	100	99.8	99.8	100	99.9
Open circuit (OC)	100	99.0	99.5	100	99.6	99.8
Gain (G)	99.7	97.8	98.7	99.9	98.9	99.4
Offset (OFF)	100	98.3	99.1	99.5	99.0	99.2
Saturation (SAT)	99.8	99.0	99.4	99.9	99.6	99.7
Macro average	99.8	98.8	99.3	99.8	99.4	99.6
Weighted average	99.6	99.6	99.6	99.8	99.8	99.8
Accuracy	99.6			99.8		

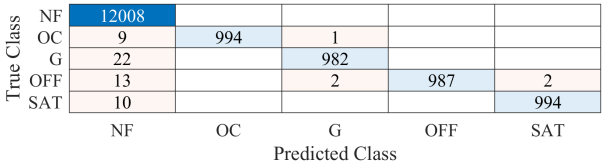

(a)

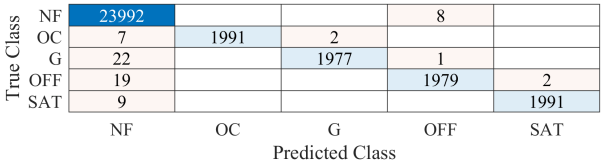

(b)

Fig. 9. Confusion matrices for IM (a) and PMSM (b)

damage occurred, it was correctly classified in the majority of cases, which is confirmed by the recall index values of around 99% in Table 3. The double number of data in the confusion matrices for PMSM is due to the fact that the rated frequency of this motor (100 Hz) is twice that of IM (50 Hz).

6. CONCLUSIONS

The presented tests confirm the applicability of the fault classifier developed for stator current sensors to AC motors of two different designs, and therefore confirm the versatility of the method. The following observations can be drawn from the simulation studies carried out:

- The accuracy of the classifier for the IM drive and the PMSM drive is comparable (99.6% for IM and 99.8% for PMSM) (Table 3). These results were obtained for tests carried out at various operating points of the drive, even at low speeds and loads (25% of the rated values).
- The neural classifier does not require retraining to operate correctly on a new object.
- The response time of the classifier depends inversely on the frequency of the first harmonic of the stator phase current.
- Synthetic data derived from the mathematical fault model accounted for 80% of the total training set. The remaining 20% was recorded in a drive system with undamaged current sensors. This compilation allowed the classifier to be independent of the operating point and motor parameters.
- An advantage of the classifier is its ability to operate in a dynamic state, as shown in Fig. 7.
- The universal classification method developed using MLP is also easy to implement, and due to the small structure of the neural network, it does not require significant computing power. This property can be important in the case of implementation on a physical controller.

Future research will focus on implementing the system on a laboratory bench with a PMSM, as well as ensuring the reliability of the method's performance in the case of changes in machine parameters due to thermal effects.

APPENDIX

Table 4
Rated parameters of the AC motors tested

Rated parameters	IM	PMSM
Voltage [V]	230	325
Current [A]	2.5	6.6
Speed [r/min]	1390	1500
Torque [N·m]	7.56	16
Pole pairs [–]	2	4
Rotor winding resistance [Ω]	4.968	–
Stator winding resistance [Ω]	5.114	1.206
Rotor leakage inductance [mH]	31.6	–
Stator leakage inductance [mH]	31.6	–
Main inductance [mH]	541.7	–
Stator inductance [mH]	–	27.58
Mutual inductance [mH]	–	7.02

ACKNOWLEDGEMENTS

This work was supported by the National Science Centre, Poland, under Grant 2021/41/B/ST7/02971.

REFERENCES

[1] D.U. Campos-Delgado, D.R. Espinoza-Trejo, and E. Palacios, "Fault-tolerant control in variable speed drives: a survey," *IET Electr. Power Appl.*, vol. 2, no. 2, pp. 121–134, Mar. 2008, doi: 10.1049/iet-epa:20070203.

[2] M. Blanke, M. Staroswiecki, and N.E. Wu, "Concepts and methods in fault-tolerant control," in *Proc. 2001 American Control Conference*, USA, 2001, pp. 2606–2620 vol. 4, doi: 10.1109/ACC.2001.946264.

[3] Y. Liu, M. Stettenbenz, and A.M. Bazzi, "Smooth Fault-Tolerant Control of Induction Motor Drives With Sensor Failures," *IEEE Trans. Power Electron.*, vol. 34, no. 4, pp. 3544–3552, Apr. 2019, doi: 10.1109/tpel.2018.2848964.

[4] K. Teler, M. Skowron, and T. Orłowska-Kowalska, "Implementation of MLP-Based Classifier of Current Sensor Faults in Vector-Controlled Induction Motor Drive," *IEEE Trans. Ind. Inform.*, vol. 20, no. 4, pp. 5702–5713, April 2024, doi: 10.1109/TII.2023.3336348.

[5] K.-S. Lee and J.-S. Ryu, "Instrument fault detection and compensation scheme for direct torque controlled induction motor drives," *IEE Proc.-Control Theory Appl.*, vol. 150, no. 4, pp. 376–382, Jul. 2003, doi: 10.1049/ip-cta:20030596.

[6] C. Chakraborty and V. Verma, "Speed and Current Sensor Fault Detection and Isolation Technique for Induction Motor Drive Using Axes Transformation," *IEEE Trans. Ind. Electron.*, vol. 62, no. 3, pp. 1943–1954, Mar. 2015, doi: 10.1109/tie.2014.2345337.

[7] T.A. Najafabadi, F.R. Salmasi, and P. Jabehdar-Maralani, "Detection and Isolation of Speed-, DC-Link Voltage-, and Current-Sensor Faults Based on an Adaptive Observer in Induction-Motor Drives," *IEEE Trans. Ind. Electron.*, vol. 58, no. 5, pp. 1662–1672, May 2011, doi: 10.1109/tie.2010.2055775.

[8] M. Adamczyk and T. Orlowska-Kowalska, "Virtual Current Sensor in the Fault-Tolerant Field-Oriented Control Structure of an Induction Motor Drive," *Sensors*, vol. 19, no. 22, p. 4979, Nov. 2019, doi: 10.3390/s19224979.

[9] M. Adamczyk and T. Orlowska-Kowalska, "Postfault Direct Field-Oriented Control of Induction Motor Drive Using Adaptive Virtual Current Sensor," *IEEE Trans. Ind. Electron.*, vol. 69, no. 4, pp. 3418–3427, April 2022, doi: 10.1109/TIE.2021.3075863.

[10] M. Skowron, E. Jamshidpour, K. Teler, T. Orlowska-Kowalska, and P. Haghgooei, "Current sensor fault detection and compensation system for wound rotor synchronous motor based on neural networks," in *2023 IEEE Transportation Electrification Conference and Expo, Asia-Pacific (ITEC Asia-Pacific)*, Thailand, 2023, pp. 1–5, doi: 10.1109/ITECAsia-Pacific59272.2023.10372315.

[11] C. Attaianese, M. D'Arpino, M.D. Monaco, and L.P. Di Noia, "Modeling and Detection of Phase Current Sensor Gain Faults in PMSM Drives," *IEEE Access*, vol. 10, pp. 80106–80118, 2022, doi: 10.1109/access.2022.3195025.

[12] H.I. Fawaz, G. Forestier, J. Weber, L. Idoumghar, and P.-A. Muller, "Deep Neural Network Ensembles for Time Series Classification," in *2019 International Joint Conference on Neural Networks (IJCNN)*, Budapest, Hungary, 2019, pp. 1–6, doi: 10.1109/IJCNN.2019.8852316.

[13] M.-F. Guo, N.-C. Yang, and W.-F. Chen, "Deep-Learning-Based Fault Classification Using Hilbert–Huang Transform and Convolutional Neural Network in Power Distribution Systems," *IEEE Sens. J.*, vol. 19, no. 16, pp. 6905–6913, Aug. 2019, doi: 10.1109/jsen.2019.2913006.

[14] J.-H. Shim, J. Lee, and J.-I. Ha, "Current-Sensor and Switch-Open Fault Diagnosis Based on Discriminative Machine Learning Model for PMSM Driving System," in *2021 IEEE Energy Conversion Congress and Exposition (ECCE)*, Canada, Oct. 2021, pp. 5098–5104, doi: 10.1109/ecce47101.2021.9595123.

[15] A.A. Silva, A.M. Bazzi, and S. Gupta, "Fault diagnosis in electric drives using machine learning approaches," in *2013 International Electric Machines & Drives Conference*, Chicago, USA, 2013, pp. 722–726, doi: 10.1109/IEMDC.2013.6556173.

[16] M. Skowron and C.T. Kowalski, "Permanent Magnet Synchronous Motor Fault Detection System Based on Transfer Learning Method," in *IECON 2022 – 48th Annual Conference of the IEEE Industrial Electronics Society*, Brussels, Belgium, 2022, pp. 1–6, doi: 10.1109/IECON49645.2022.9968867.

[17] S. Ziegler, R.C. Woodward, H.H.-C. Iu, and L.J. Borle, "Current Sensing Techniques: A Review," *IEEE Sens. J.*, vol. 9, no. 4, pp. 354–376, Apr. 2009, doi: 10.1109/jsen.2009.2013914.

[18] M.P. Kazmierkowski, R. Krishnan, and F. Blaabjerg, *Control in Power Electronics – Selected Problems*. USA, 2002.

[19] Y. Azzoug, M. Sahraoui, R. Pusca, T. Ameid, R. Romary, and A.J.M. Cardoso, "A Variable Speed Control of Permanent Magnet Synchronous Motor Without Current Sensors," in *020 IEEE 29th International Symposium on Industrial Electronics (ISIE)*, Delft, Netherlands, 2020, pp. 1523–1528, doi: 10.1109/ISIE45063.2020.9152572.